3D Printed Microfluidic Device with Integrated Biosensors for Online Analysis of Subcutaneous Human Microdialysate.

Gowers, SA; Curto, VF; Seneci, CA; Wang, C; Anastasova, S; Vadgama, P; Yang, GZ; Boutelle, MG

analytical chemistry

Article

pubs.acs.org/ac

3D Printed Microfluidic Device with Integrated Biosensors for Online Analysis of Subcutaneous Human Microdialysate

Sally A. N. Gowers,[∥,†] Vincenzo F. Curto,[∥,‡] Carlo A. Seneci,[‡] Chu Wang,[†] Salzitsa Anastasova,[§] Pankaj Vadgama,[§] Guang-Zhong Yang,[‡] and Martyn G. Boutelle*[,†]

[†]Department of Bioengineering and [‡]The Hamlyn Centre, Imperial College London, London SW7 2AZ, United Kingdom

[§]School of Engineering and Materials Science, Queen Mary, University of London, Mile End Road, London E1 4NS, United Kingdom

Supporting Information

ABSTRACT: This work presents the design, fabrication, and characterization of a robust 3D printed microfluidic analysis system that integrates with FDA-approved clinical microdialysis probes for continuous monitoring of human tissue metabolite levels. The microfluidic device incorporates removable needle type integrated biosensors for glucose and lactate, which are optimized for high tissue concentrations, housed in novel 3D printed electrode holders. A soft compressible 3D printed elastomer at the base of the holder ensures a good seal with the microfluidic chip. Optimization of the channel size significantly improves the response time of the sensor. As a proof-of-concept study, our microfluidic device was coupled to lab-built wireless potentiostats and used to monitor real-time subcutaneous glucose and lactate levels in cyclists undergoing a training regime.

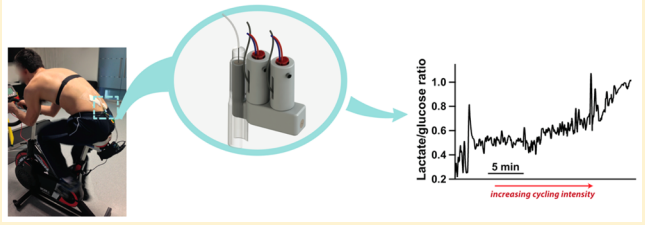

Wearable sensors connected to body sensor networks (BSN)[1] that provide real-time information about the wearer's health and fitness[2] are of great interest both academically and commercially. Developments of such platforms have mainly focused on sensors that measure physical vital signs (e.g. pulse rate, ECG). Biosensors targeting physiologically relevant analytes are more challenging but can provide important information about tissue health[3] and fitness,[4,5] allowing, for example, athletes to tailor their training to their individual characteristics, enabling them to assess their training effectiveness, to make adjustments, and to track improvements in their performance.

Extensive research efforts have focused on the development of miniaturized on-body chemo/biosensors for the measurement of physiological analytes in different bodily fluids, such as interstitial fluid,[6,7] sweat,[8,9] tears,[10,11] and saliva.[12,13] Glucose and lactate are particularly attractive biomarkers to monitor as they provide information about tissue energy metabolism. Lactate, in particular, has received much interest for sports monitoring. During intense exercise, tissue oxygen levels are insufficient for aerobic metabolism to meet the energy demands of the body. Instead, anaerobic metabolism occurs to meet these increased energy demands, leading to elevated lactate levels. Lactate can therefore be used as a measure of how hard the body is working, allowing athletes to modulate their effort accordingly, in order to train the body to increase its efficiency in clearing excess lactate or to avoid causing damage by overtraining.

Commercially available blood lactate and glucose meters are used for sports applications.[14] Although blood measurements provide important information about global metabolite levels in the body, the use of finger-prick test strips has several limitations. The main limitation of discrete sampling is the lack of temporal resolution, with the result that it is not possible to observe dynamic changes in metabolite levels. In order to improve temporal resolution blood samples have to be taken regularly, resulting in constant interruptions during the activity period. In contrast, online microdialysis allows continuous monitoring of tissue metabolites, which, when coupled with an online analysis system, provides good temporal resolution, suitable for resolving dynamic changes.[15−17] The microdialysis probe consists of a semipermeable membrane that is perfused with a solution that matches the extracellular fluid. Formation of a concentration gradient across the membrane allows exchange of molecules between the probe and the tissue, creating a dialysate stream that can be analyzed for compounds of interest. Microdialysis has been used in a wide range of applications and is an attractive technology for human *in vivo* monitoring, as commercial FDA-approved probes are available. Microdialysis combined with online analysis systems has been used extensively to detect tissue health and ischemic events.[18−21] In particular, the lactate/glucose ratio has been shown to be an especially sensitive marker of tissue health, providing a clear indication as to whether tissue energy demands are being met.[16,19,22]

There is a natural synergy between microdialysis and microfluidic devices because high time resolution analysis of low volume flow rates requires very small internal

Received: April 10, 2015
Accepted: June 12, 2015
Published: June 12, 2015

DOI: 10.1021/acs.analchem.5b01353
Anal. Chem. 2015, 87, 7763−7770

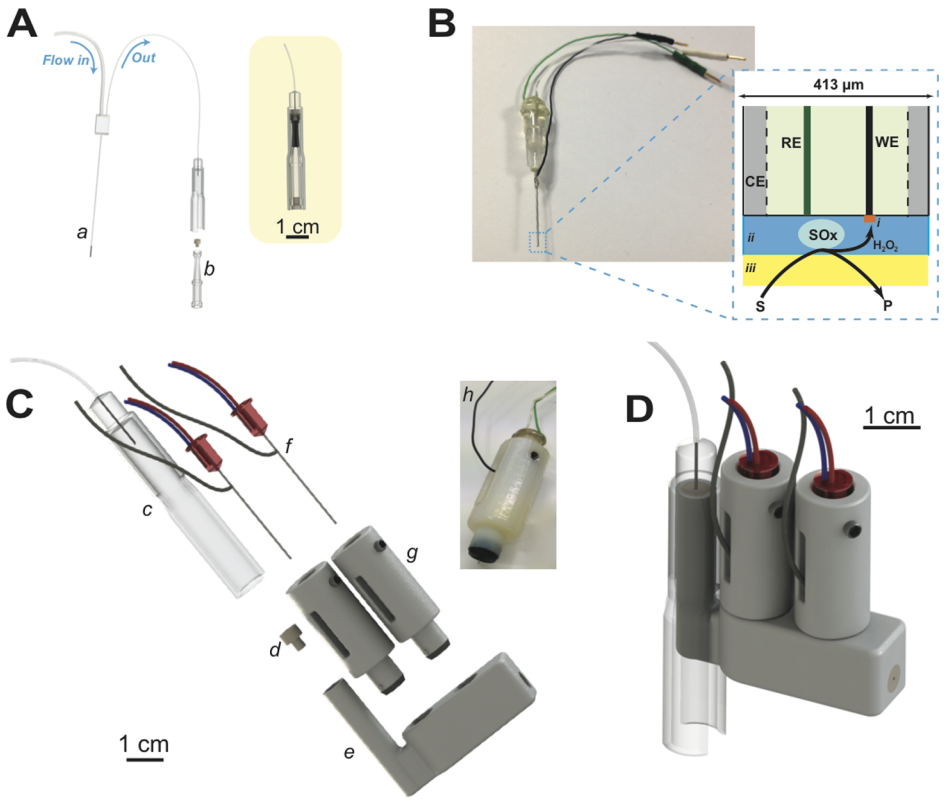

Figure 1. A. Standard microdialysis setup for discrete sampling. The probe (*a*) is perfused at a fixed low flow rate, and dialysate is collected into a microvial (*b*) at the probe outlet. *Right:* shows the microvial when connected to the probe outlet holder. B. Photograph of combined needle electrode based on a 27G hypodermic needle and schematic cross-section of the needle tip, showing the layers that make up the biosensor: *(i)* m-PD exclusion layer, *(ii)* substrate oxidase (SOx) entrapped in a hydrogel, and *(iii)* diffusion limiting polyurethane outer film. C. Exploded view of custom-made microfluidic device for continuous monitoring of dialysate, showing the multicomponent system. The microfluidic chip (*e*) connects to the probe outlet holder (*c*) in place of a microvial. The outlet holder needle enters the microvial rubber insert (*d*) at the inlet of the microfluidic chip. Glucose and lactate needle biosensors (*f*) are housed in custom-made electrode holders (*g*) that screw into the microfluidic chip, placing the biosensors in the middle of the microfluidic channel and providing a good seal between the holder and the microfluidic device. (*h*) shows a photograph of an electrode holder containing a needle biosensor. The black part at the base of the holder is made of soft, compressible plastic to ensure the holder makes a good seal with the microfluidic chip. D. The L-shaped design provides a tidy and compact overall system.

volumes.[17,20,23] Conventionally, microfluidic devices have been made using methods such as PDMS-based soft lithography due to their ease of fabrication. PDMS chips have been used extensively for proof-of-concept analysis devices for mass spectrometry,[24] as well as for optical[23,25] and electrochemical detection.[20,26,27] In all cases the analyzer is a large device placed on a bench near the experimental subject. In our current PDMS-needle biosensor system this requires >1 m of connection tubing between the probe and the PDMS chip, leading to a 25 min delay before analysis at 1 μL/min flow rate, as well as a broadened temporal response due to Taylor dispersion.[28] Furthermore, our current method for manually positioning the needle electrode biosensors inside the PDMS chamber is impractical for a wearable device as movement caused by exercise leads to repositioning of the biosensor inside the microfluidic channel leading to noise and decreased sensitivity.[27]

Fast responding wearable devices need to be small and robust and placed close to the microdialysis probe outlet.[29] For reliability, they require a robust low-volume connection to the probe and should ideally incorporate biosensors as easily replaceable modules, given the possibility of biosensor failure during high-value monitoring of athletes.

Recently, there has been great interest in the use of 3D printing for the fabrication of microfluidic devices.[30−34] This rapid prototyping methodology is particularly attractive as it enables one-step fabrication of a microfluidic platform.[35] It also enables dimensional control of the device, so that it can be integrated with commercially available components.[30] The versatility of this fabrication method allows for a flexible, modular-approach to device design with each part designed to meet exact requirements. It also allows for design modifications to be made quickly and easily so that device features can be adjusted iteratively, and their influence on the device performance can be evaluated.[30,35] Erkal et al. recently reported on the fabrication of 3D printed microfluidic devices with integrated electrodes for electrochemical detection.[30] These devices were fabricated using commercial flangeless fitting nuts to house the electrodes, which integrated with microfabricated receiving ports.

Here, we show for the first time, the development of a 3D printed microfluidic device that integrates with FDA-approved clinical microdialysis probes and incorporates needle type biosensors and which can be used for continuous monitoring of human tissue metabolite levels. As a proof-of-concept, the device is employed for online monitoring of lactate and glucose tissue levels during cycling trials, providing a robust and reliable platform with potential use for wearable sensing technologies.

DOI: 10.1021/acs.analchem.5b01353
Anal. Chem. 2015, 87, 7763−7770

EXPERIMENTAL SECTION

Reagents. Glucose oxidase (GOx) from *Aspergillus niger* and lactate oxidase (LOx) from *Aerococcus viridians* were purchased from Sekisui Diagnostics. Polyurethane (Texin 985) was obtained from Bayer. Other reagents were obtained from Sigma-Aldrich.

Electrode Fabrication. The biosensors used in this work are based on combined needle electrodes.[20,36] Briefly, a 50 μm diameter polytetrafluoroethylene (PTFE) insulated platinum/iridium (90%:10%) wire (Advent Research Materials, UK) and a 50 μm polyester insulated silver wire were threaded through a 27G hypodermic needle. The insulation layer was removed from the ends of the wires using a small flame, to expose the metal. The ends of the two wires were each connected to an electrical wire using conductive silver epoxy glue (RS Components, UK). Epoxy resin (Robnor resins, CY1301 and HY1300) was used to fill the needle and to secure the wires in place. Once the epoxy resin was cured, the sharp tip of the needle was abraded using sandpaper (Buehler, UK), to just above the bevel of the needle, to create silver and platinum disc electrodes. The blunt needle was then polished sequentially with alumina slurries (1, 0.3, and 0.05 μm). Finally, in order to create the AglAgCl reference electrode, the tip of the needle was dipped into a potassium dichromate reference solution (BASi, US) for 3 s, and then into a solution of diluted 37% hydrochloric acid for 20 s, to remove the oxide layer from the working and auxiliary electrodes. Cyclic voltammetry was used to assess the working electrode surface.

Biosensor Fabrication. All biosensors were controlled using in-house potentiostats and a PowerLab 8/35, controlled by LabChart Pro (ADInstruments). Glucose and lactate biosensors were fabricated in several layers, as shown in Figure 1-B. *Layer i:* The working electrode was first coated with poly m-phenylenediamine (m-PD) using electropolymerization, to screen out potential interferences. Briefly, the combined needle electrode was placed in a 100 mM solution of m-phenylenediamine in 0.01 M PBS at pH 7.4. The potential was held at 0 V for 20 s, 0.7 V for 20 min for electropolymerization to occur, and then 0 V for 5 min. The electrode was gently rinsed with deionized water, and cyclic voltammetry was used to verify that the working electrode had been successfully coated. *Layer ii:* After successful electropolymerization of the screening layer, the electrodes were dipped into the enzyme solution (60 mg/mL LOx or GOx, 30 mg/mL bovine serum albumin, 60 mg/mL poly(ethylene glycol) diglycidyl ether, and 2% *v/v* glycerol in 0.01 M PBS, adapted from the method described by Vasylieva et al.[37,38]). The needles were placed in an oven at 55 °C for 2 h. *Layer iii:* Following enzyme immobilization, biosensors were also coated with a polyurethane film in order to extend their dynamic range to include the higher lactate levels possible in exercising tissue and to minimize the effect of any flow variations, which could occur in a flow-cell, on biosensor response.

Fabrication of Microfluidic Platform. Two different 3D printers were used for printing of the microfluidic platform. The microfluidic chip was fabricated using a 3D printer ULTRA 3SP. This machine provides 100 μm resolution in the *X*- and *Y*-axis and between 25 and 100 μm resolution in the *Z*-axis, depending on the parameters set. However, the true resolution of the printer is given by the voxel dimension and the material employed during fabrication. Throughout the development of this work, the "ABS 3SP White" resist was used for printing of the microfluidic chip. ABS 3SP White allows printing of dimensionally and mechanically stable components, although due to shrinkage of the resist in the printing process smaller dimensions than those specified in the design of the microfluidic channel were observed. In general, a tolerance of about 100 μm needs to be considered during the design of the components. The microfluidic platform was designed with an L-shape, in which the inner microfluidic channel incorporates a 90° bend (Figure S1-A). As the microfluidic chip needs to integrate two separate needle biosensors, one for glucose and the other for lactate sensing, it was decided to insert the two needles into the microfluidic channel through two round openings printed on the top wall of the microchannel (Figure S1-C). This configuration ensures a tidy and compact packaging of the overall platform, as shown in Figure 1-j. However, it limits the minimum microchannel width that is achievable, as it has to fit the 27G needle (Ø = ca. 413 μm) biosensors. Three different sizes of microfluidic channels were printed and tested, which had different height and width dimensions, these were as follows: (1) 520 × 520 μm, (2) 750 × 550 μm, and (3) 1000 × 550 μm. Moreover, taking into account the material shrinkage, for channel (1) two slightly wider microfluidic chambers were designed at the two needle biosensor insertion locations (Figure S1-B) to avoid issues during placement of the biosensors.

Printing of the needle holders was performed using the Objet260 Connex 3D printer. The main advantage of using this printer compared to the ULTRA 3SP is the possibility to print rigid and soft material simultaneously on the same component. For instance, VeroWhitePlus (RGD835) and TangoBlack (FLX973) were employed for the printing of the rigid and soft parts, respectively. To fix the position of the needle biosensor inside the holder two grub screws M2.5 were also used. The rubbery part of the holder has a truncated cone shape to guarantee fluidic sealing and to avoid incorrect positioning of the biosensors inside the microfluidic channel. In fact, initial attempts using a cylindrical shape rubber part lead to incorrect mounting of the biosensor holder into the microfluidic chip due to XY expansion of the rubber when compressed.

Calibration and Characterization Studies. Glucose and lactate biosensors were both held at a constant potential of +0.7 V vs AglAgCl. The biosensors were calibrated inside the microfluidic chip using a calibration board, consisting of two LabSmith 20 μL programmable syringe pumps, one containing T1 perfusion solution and one containing a glucose/lactate standard. By mixing the flows, a multipoint calibration was carried out by varying the relative flow rates of the two pumps, while keeping the overall flow rate constant at 1 μL/min. This system was also used to measure the time response of the biosensors in the microfluidic chip, by switching between the two solutions and measuring the time taken for the sensors to reach a steady current. *In vitro* microdialysis experiments were conducted using an expired microdialysis probe (CMA70, MDialysis, 10 mm membrane length, 20 kDa molecular-weight cutoff), perfused with T1 solution (2.3 mM calcium chloride, 147 mM sodium chloride, and 4 mM potassium chloride) at 1 μL/min using a microdialysis pump (CMA107, MDialysis).

Cycling Protocol. For *in vivo* microdialysis experiments, all procedures were approved by the local ethics committee (NRES 10/H0808/124, protocol CRO1608), and probes were inserted percutaneously by a qualified clinician. The skin was cleaned with alcohol wipes, and an anesthetic cream (EMLA, APP Pharmaceuticals) was applied to the skin 45 min prior to

DOI: 10.1021/acs.analchem.5b01353
Anal. Chem. 2015, 87, 7763−7770

probe insertion. An ice pack was also placed on the skin 5 min before probe insertion, to further numb the area. A sterile CMA63 microdialysis probe (Mdialysis, 10 mm membrane length, 20 kDa molecular-weight cutoff) was inserted subcutaneously, using the tunnelling needle and introducer supplied, and secured in place with 3M single coated conformable incise medical tape. The probe was perfused with sterile T1 perfusion solution (MDialysis) at 1 μL/min using a microdialysis pump (CMA107, MDialysis). Prior to beginning exercise, baseline dialysate levels of glucose and lactate were measured. The cycling protocol consisted of 3 levels of increasing intensity, followed by a 1 min sprint, and finally a warm-down phase, as shown in Figure 4-A. Dialysate glucose and lactate levels were also recorded during the recovery phase immediately after exercise.

Cycling trials were performed using a Wattbike (Wattbike, UK), that allows recording of pedal cadence (rpm) and heart rate using a wireless chest belt (Sunto dual chest belt). Data was despiked,[39] and the time delay between the microdialysis probe and the analysis system removed. Current measurements were converted into concentration values using pre-experiment calibrations.

RESULTS AND DISCUSSION

3D Printed Microfluidic Device. The design of the 3D printed microfluidic device was driven by the need to make a reliable and simple connection between the microfluidic chip and the commercially available microdialysis probe through the use of the probe outlet holder (Figure 1-C item c). This simplifies the overall device architecture, as no extra connection tubing and adaptors are needed, additionally decreasing the overall dead volume of the system.

The design of the microfluidic device was inspired by the configuration used in the standard microdialysis setup (Figure 1-A), in which the microfluidic device slots into the probe outlet holder and replaces the microvial, as shown in Figure 1-D. To achieve this, the microfluidic chip (Figure 1-C item e) was designed and printed with a unique *L*-shape, the vertical arm for connection purposes and the horizontal arm for integration of the two needle biosensors. The vertical arm of the chip presents similar geometry to the microvial. For instance, the microfluidic inlet port was printed to incorporate the rubber insert (Figure 1-C item d) from the microvial, so as to take advantage of the easy and leak-free connection port. Moreover, this design offers flexibility for the device to be used in a diverse range of microdialysis applications, as it can be used with all clinical microdialysis probes, since they have the same type of outlet holder.

With regard to the horizontal section of the microfluidic device, a major challenge was to incorporate and secure the biosensors in the correct position inside the microfluidic channel, preventing any leaks. Initially, attempts were made to achieve this by threading the needle electrode through a commercially available 1/32″ one-piece fitting (2-56 UNC) and using this to secure the electrode in place inside the microfluidic chip.[30] Using this approach, the device dimensions were determined by the size of the fittings and as such were relatively large (over 1 mm). However, integrating the biosensor in this way did not provide a good seal with the microfluidic chip, causing leaks to occur. Erkal et al. showed that electrodes could be successfully integrated with 3D printed microfluidic devices using commercially available fittings; however, due to the small size of our sensor, a 1/32″ fitting was required. These threads were too small (2-56 UNC) to be printed and a thread tapping tool (M2.5) was used instead. Unfortunately this approach did not provide a satisfactory seal or good reproducibility. To overcome the issue of the previous method, custom-made electrode holders (Figure 1-C parts g and h) were also designed and 3D printed, which allow better control over the electrode placement inside the microfluidic channel.

The electrode holder was printed using the Objet260 Connex 3D printer, capable of printing both hard and soft plastics simultaneously on the same component. This enabled the bottom part of the holder to be printed using a soft and compressible plastic, ensuring a good seal between the holder and the microfluidic device, preventing potential leaks. The holders were designed so that the needle tip protruded from the end and the needle was secured in place using two grub screws. The needle position inside the holder could be varied depending on the length of the needle, as this can change after repeated polishing of the electrode (see supporting video 1).

This ensures that the needle tip is at a fixed distance from the end of the holder and hence in the correct position inside the microfluidic channel. The microfluidic platform was designed so that the holder could be guided into position; two pegs on the sides of the electrode holder inserted into guiding slots and locked into place, positioning the needle tip precisely inside the channel (see supporting video 2). Moreover, to facilitate the positioning of the electrode inside the microchannel an additional cross-sectional cut-out of the microfluidic device was printed. Using the cut-out component it was possible to visualize the electrode inside the channel under a microscope and to precisely secure the sensors inside the holders so that the tip of the biosensor was at the desired height inside the microchannel (Figure S2).

The use of 3D printing for fabrication of the device enabled a modular approach to be adopted, designing separate parts to be integrated together. Using this method each part of the device could be designed and optimized iteratively to meet its own individual requirements.

Biosensor Characterization Inside 3D Printed Microfluidic Chip. To investigate the effect of the microfluidic channel dimensions on the response time of the sensors, three different channel sizes were tested, as described in the Experimental Section. Figure 2-B shows the normalized current response of a glucose biosensor to a step change from 0 to 2 mM at 1 μL/min for the different channel sizes. In each case the sensor was positioned in the middle of the channel. Cross sections of each channel were measured using a microscope to determine the actual dimensions of each of the channels. The dimensions specified in the table in Figure 2-B refer to the measured dimensions.

Both glucose and lactate biosensors without the polyurethane (PU) outer film are fast responding (for a step change in well-stirred beaker T_{90} glucose = 6.6 ± 3.9 s (n = 24), lactate = 5.1 ± 2.6 s (n = 30), data not shown). Addition of the PU film to extend the dynamic range (necessary for lactate biosensor) slows both sensors (as shown in Figure 2-A) and increases the variability in response as the PU thickness is difficult to control (for a step change T_{90} glucose = 36.1 ± 19.6 s (n = 5), lactate = 22.8 ± 11.3 s (n = 21)). The same biosensor shows good reproducibility. For example, the sensors in Figure 2-A have T_{90} glucose = 21.0 ± 0.6 s (n = 3) and lactate = 26.1 ± 1.4 s (n = 3). Laminar flow inside the connection tubing and microfluidic channel leads to broadening of the concentration change, due

DOI: 10.1021/acs.analchem.5b01353
Anal. Chem. 2015, 87, 7763−7770

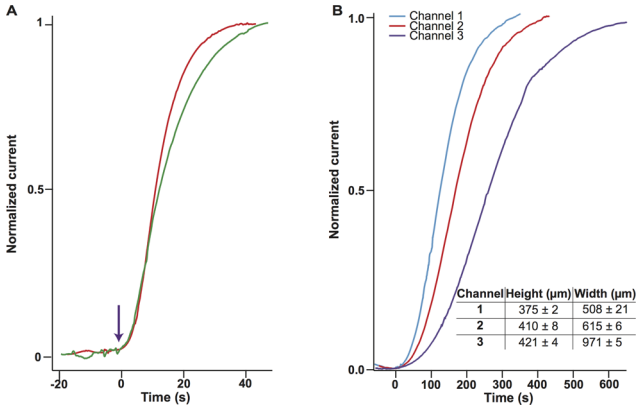

Figure 2. A. Normalized current response of a 50 μm disc glucose (red) and lactate (green) biosensor in a stirred beaker to a 2 mM concentration step (purple arrow). B. The graph shows the normalized current for a glucose biosensor to a step change from 0 to 2 mM at 1 μL/min in three different microfluidic channels. The measured channel sizes are shown in the table inset. The response time increases as the channel dimension increases.

to Taylor dispersion.[28] In Figure 2-B we show that the time response of the sensor to a step change is reduced by decreasing the channel cross-sectional area. The T_{90} values are summarized in Table 1 and are generally inversely proportional

Table 1. Effect of Channel Size on Response Time

channel dimensions H × W (μm)	glucose T_{90} (s)	lactate T_{90} (s)
375 × 508	208 ± 6.5	194 ± 15
410 × 615	267 ± 7.7	227 ± 7.0
421 × 971	398 ± 12.8	286 ± 6.9

to cross-sectional area and hence proportional to linear flow rate. In the channel, glucose values are longer than lactate ones because the glucose biosensor was second in line and hence exposed to a greater channel volume. The fastest response time was observed in channel 1; therefore, these dimensions were chosen for the final device.

The horizontal section of the microfluidic chip is similar to the microfluidic device described by Erkal et al., which had an internal volume of 3.90 μL. Our microfluidic chip is broadly similar, but the internal volume up until the first biosensor is approximately 1.91 μL based on measured dimensions.

Metabolite levels in tissue vary between people and depend on a person's metabolism and fitness during exercise, as well as on the particular tissue being sampled.[40] The system was calibrated online from 0 to 10 mM, at 1 μL/min to verify that it is capable of detecting physiologically relevant concentrations of glucose and lactate levels in the dialysate. Figure 3 shows typical current response vs concentration for the biosensors when placed in the microfluidic device. These data indicate that the biosensing system has good sensitivity to glucose and lactate, with clear current changes corresponding to increasing levels of substrate. The biosensors show a good dynamic range, suitable for physiological monitoring. The fact that sensitivities are similar for the glucose and lactate sensors (Figure 3) reflects the mass-transport limiting effects of the PU membrane.

As a further validation test, it was important to test the microfluidic device with a microdialysis probe *in vitro*. To mimic changes occurring in the tissue, the microdialysis probe was placed in a well-stirred beaker and subjected to changes in

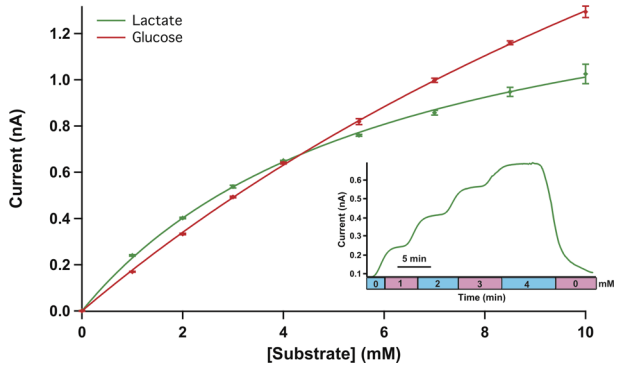

Figure 3. Typical calibration curves for 50 μm disc glucose and lactate biosensors in the microfluidic device at 1 μL/min. Mean ± standard deviation of measurement shown (n = 4). Points fitted with the Michaelis–Menten equation. Inset: Raw data for a typical 5-point lactate calibration from 0 to 4 mM in 1 mM steps.

beaker lactate and glucose concentrations. The outlet holder of the microdialysis probe was connected to the microfluidic device, which continuously measured the glucose and lactate levels of the dialysate.

As the biosensors are placed consecutively in the microfluidic chip, there is a 2 min delay between the lactate and glucose responses to the dialysate changes. There is also an additional delay to take into account between the changes occurring at the probe membrane and the analysis system due to the length of outlet tubing. Taking both factors into consideration, the total delay was found to be 13 min for the lactate biosensor, which was placed first in the direction of flow and 15 min for the glucose biosensor, which was placed second in the direction of flow. This delay is largely caused by the commercially available probe outlet tubing and, therefore, could be reduced further still if the extension on the probe outlet was shortened. Nevertheless, the delay time of the microfluidic device described here was substantially improved compared to our PDMS-based microfluidic device, which had a lag time of 25 min using the same flow rate (1 μL/min).

Online Subcutaneous Glucose and Lactate Measurement during Cycling Trials. In a proof-of-concept study to demonstrate the potential of this device for continuous monitoring applications the 3D printed microfluidic chip, housing glucose and lactate needle biosensors, was tested as a wearable device for online measurement of subcutaneous metabolite levels during cycling training in two cyclists.

Following probe insertion, the microfluidic device was connected to the probe outlet holder and secured to the lower back, as shown in Figure 4-A. The biosensors were connected to an in-house wireless potentiostat, housed inside a saddlebag attached to the bike seat. The wireless potentiostat used was relatively large (10.5 × 6.0 × 5.0 cm L × W × H) compared to the microfluidic device and is not yet small enough to be integrated into a fully wearable system. Current research within our groups is aimed at miniaturization of this device.

A schematic of the cycling protocol is shown in Figure 4-B. Baseline glucose and lactate levels were measured in the dialysate, following probe insertion, prior to exercise. The exercise phase consisted of three levels of increasing intensity, followed by a short sprint and a period of warming down. Finally, dialysate glucose and lactate levels were monitored during the recovery period following exercise.

DOI: 10.1021/acs.analchem.5b01353
Anal. Chem. 2015, 87, 7763–7770

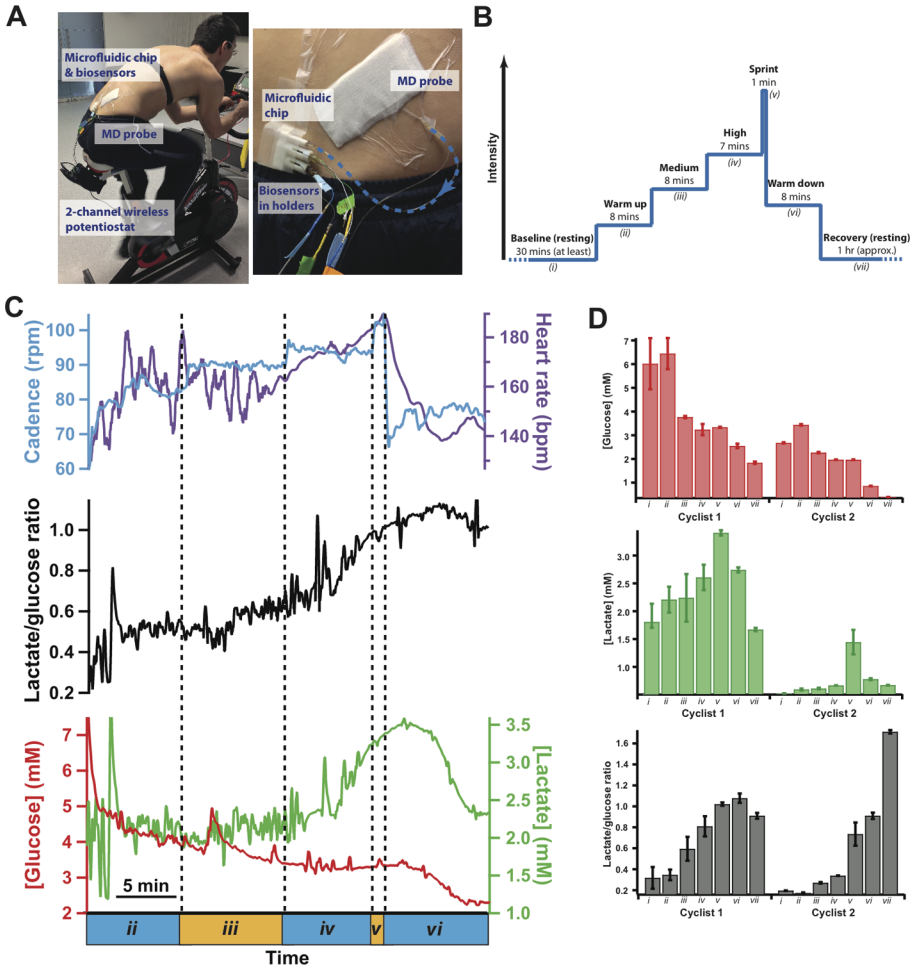

Figure 4. A. Photograph of microfluidic device to measure tissue glucose and lactate levels in dialysate during the cycling protocol. Dialysate flowed into the microfluidic chip, housing the glucose and lactate biosensors, which were connected to wireless potentiostats, secured onto the bike. B. Experimental protocol. Tissue levels were monitored during an initial resting period (*i*), followed by cycling at 4 levels of increasing rpm (*ii-v*), a level of warming down (*vi*), and a final period of resting (*vii*). C. Dialysate glucose and lactate levels during the exercise phase of the cycling protocol. The bottom graph shows the glucose (red) and lactate (green) levels, the middle graph (black) shows the lactate/glucose ratio, and the top graph shows the rotations per minute (blue) and heart rate (purple) throughout the cycling protocol. Glucose and lactate traces have been despiked.[39] The dotted lines indicate the stages of varying cycling intensity: (*ii*) 55 rpm, (*iii*) 65 rpm, (*iv*) 75 rpm, (*v*) sprint, and (*vi*) 55 rpm. Data has been time-aligned, taking into account the time delay of the system. D. Histograms showing mean dialysate levels for two different cyclists during key points in cycling protocol. Labels correspond to stages described in the experimental protocol: (*i*) baseline (*ii*) midway through warm up, (*iii*) midway through medium intensity, (*iv*) midway through high intensity, (v) end of sprint, (*vi*) end of warm down, and (*vii*) after 50 min of recovery.

Initial levels after probe insertion were variable due to the trauma of insertion. Therefore, baseline levels were monitored for at least 30 min to allow time for the tissue to stabilize following probe insertion; typically this occurred 12 min after insertion.[21]

Results obtained from one of the cyclists during the exercise phase of the cycling protocol are presented in Figure 4-C, together with data recorded using the exercise bicycle, showing heart rate and rotations per minute (rpm), to quantify the exercise intensity. Initially, during phases *ii* and *iii* the heart rate signal was noisy as there was insufficient sweat to ensure good contact between the skin and the wireless chest belt electrodes. Prior to starting exercise, baseline glucose and lactate levels in the dialysate were 6.02 ± 1.08 mM and 1.81 ± 0.33 mM, respectively (mean ± standard deviation over 30 s time period). Measured subcutaneous glucose levels decreased with increasing exercise intensity, and local levels were driven down further still following exercise, even after 50 min of rest. In contrast, lactate levels increased with increasing exercise intensity, peaking immediately after the sprint, and gradually decreased once cycling had stopped. After 50 min of resting, dialysate glucose and lactate levels were 1.84 ± 0.05 mM and 1.67 ± 0.03 mM, respectively.

To guard against possible changes in probe recovery, a ratio of the two metabolites was also calculated. The lactate/glucose ratio increased with exercise and rose more steeply with increasing cycling intensity. Interestingly, the lactate/glucose ratio continued to increase considerably, even after exercise had stopped.

An overview of the dialysate glucose and lactate levels and the lactate/glucose ratio throughout the cycling protocol for two cyclists is shown in Figure 4-D. The overall trends in glucose and lactate levels are similar for the two cyclists, although the absolute concentrations appear quite different. This variability could be caused by changes in probe recovery or by differences in the fitness levels of the cyclists. In principle, level changes caused by differences in probe recovery would have been removed using ratios of analyte concentrations, such

DOI: 10.1021/acs.analchem.5b01353
Anal. Chem. 2015, 87, 7763−7770

as the lactate/glucose ratio.[16] Such ratios are widely used for monitoring in the injured human brain (lactate/pyruvate)[41] and in muscle (lactate/pyruvate and lactate/glucose),[42] though this needs to be further investigated for subcutaneous tissue. Nevertheless, there are clear differences in the lactate/glucose ratio trend for the two cyclists.

CONCLUSION

We have demonstrated the first example of a 3D printed microfluidic device with integrated removable biosensors that joins directly to a clinical microdialysis probe for continuous human monitoring applications. Here we have demonstrated its capabilities as a wearable device for subcutaneous monitoring of tissue glucose and lactate levels in cyclists during exercise. The clear changes recorded in the local glucose and lactate levels indicate that this device could have huge potential for monitoring and evaluating athlete training effectiveness in real-time. Moreover, this miniaturized device also has potential for clinical microdialysis applications, such as bedside monitoring, as its wearable nature removes the need for long connection tubing, which usually leads to long lag times. Due to the dimensional control provided by 3D printing, it was possible to design the microfluidic device so that it could easily be integrated with commercially available microdialysis probes, making it suitable for numerous potential applications. Future work will focus on miniaturization of the wireless potentiostats to enable integration of the electronics within the wearable device. Due to the modular nature of the device, the platform can be expanded to include monitoring of other clinically relevant biomarkers, offering promise in a wide range of clinical and fitness applications.

ASSOCIATED CONTENT

Supporting Information

Additional information as noted in text (Figures S1−S3 and supporting videos 1 and 2). The Supporting Information is available free of charge on the ACS Publications website at DOI: 10.1021/acs.analchem.5b01353. Data supporting this publication can be obtained on request from biomedicalsensor@imperial.ac.uk.

AUTHOR INFORMATION

Corresponding Author

*E-mail: m.boutelle@imperial.ac.uk.

Author Contributions

‖S.G. and V.F.C. contributed equally to this work.

Notes

The authors declare no competing financial interest.

ACKNOWLEDGMENTS

We thank the EPSRC (EP/H009744/1) and Wellcome Trust DOH (HICF-0510-080) for funding. We would like to thank Mr. Vassilios Kontojannis and Mr. Hani Marcus for their expertise in carrying out the microdialysis probe insertion. We are grateful to 3M for supplying the single coated conformable incise medical tape.

REFERENCES

(1) *Body Sensor Networks*; Yang, G.-Z., Ed.; Springer: 2014.
(2) Matzeu, G.; Florea, L.; Diamond, D. *Sens. Actuators, B* **2015**, *211*, 403−418.
(3) Rogers, M. L.; Boutelle, M. G. *Annu. Rev. Anal. Chem.* **2013**, *6*, 427−453.
(4) Diamond, D.; Coyle, S.; Scarmagnani, S.; Hayes, J. *Chem. Rev.* **2008**, *108*, 652−679.
(5) Windmiller, J. R.; Wang, J. *Electroanalysis* **2013**, *25*, 29−46.
(6) Woderer, S.; Henninger, N.; Garthe, C. D.; Kloetzer, H. M.; Hajnsek, M.; Kamecke, U.; Gretz, N.; Kraenzlin, B.; Pill, J. *Anal. Chim. Acta* **2007**, *581*, 7−12.
(7) Facchinetti, A.; Sparacino, G.; Cobelli, C. *J. Diabetes Sci. Technol.* **2007**, *1*, 617−623.
(8) Curto, V. F.; Fay, C.; Coyle, S.; Byrne, R.; O'Toole, C.; Barry, C.; Hughes, S.; Moyna, N.; Diamond, D.; Benito-Lopez, F. *Sens. Actuators, B Chem.* **2012**, *171−172*, 1327−1334.
(9) Jia, W.; Bandodkar, A. J.; Valde, G.; Windmiller, J. R.; Yang, Z.; Ram, J.; Chan, G.; Wang, J. *Anal. Chem.* **2013**, *85*, 6553−6560.
(10) Kabilan, S.; Ph, D.; Lowe, C. *Diabetes Technol. Ther.* **2006**, *8*, 89−93.
(11) Iguchi, S.; Kudo, H.; Saito, T.; Ogawa, M.; Saito, H.; Otsuka, K.; Funakubo, A.; Mitsubayashi, K. *Biomed. Microdevices* **2007**, *9*, 603−609.
(12) Yoda, K.; Shimazaki, K.; Ueda, Y.; Ann, N. Y. *Acad. Sci.* **1998**, *864*, 600−604.
(13) Mannoor, M. S.; Tao, H.; Clayton, J. D.; Sengupta, A.; Kaplan, D. L.; Naik, R. R.; Verma, N.; Omenetto, F. G.; McAlpine, M. C. *Nat. Commun.* **2012**, *3*, 763.
(14) Krustrup, P.; Mohr, M.; Steensberg, A.; Bencke, J.; Kjaer, M.; Bangsbo, J. *Med. Sci. Sports Exercise* **2006**, *38*, 1165−1174.
(15) Watson, C. J.; Venton, B. J.; Kennedy, R. T. *Anal. Chem.* **2006**, *78*, 1391−1399.
(16) Parkin, M. C.; Hopwood, S. E.; Boutelle, M. G.; Strong, A. J. *TrAC, Trends Anal. Chem.* **2003**, *22*, 487−497.
(17) Schultz, K. N.; Kennedy, R. T. *Annu. Rev. Anal. Chem.* **2008**, *1*, 627−661.
(18) Nandi, P.; Lunte, S. M. *Anal. Chim. Acta* **2009**, *651*, 1−14.
(19) Rogers, M. L.; Brennan, P. A.; Leong, C. L.; Gowers, S. A. N.; Aldridge, T.; Mellor, T. K.; Boutelle, M. G. *Anal. Bioanal. Chem.* **2013**, *405*, 3881−3888.
(20) Rogers, M. L.; Feuerstein, D.; Leong, C. L.; Takagaki, M.; Niu, X.; Graf, R.; Boutelle, M. G. *ACS Chem. Neurosci.* **2013**, *4*, 799−807.
(21) Deeba, S.; Corcoles, E. P.; Hanna, G. B.; Hanna, B. G.; Pareskevas, P.; Aziz, O.; Boutelle, M. G.; Darzi, A. *Dis. Colon Rectum* **2008**, *51*, 1408−1413.
(22) Birke-Sorensen, H. *J. Transplant.* **2012**, *2012*, 970630.
(23) Wang, M.; Roman, G. T.; Schultz, K.; Jennings, C.; Kennedy, R. T. *Anal. Chem.* **2008**, *80*, 5607−5615.
(24) Sun, S.; Slaney, T. R.; Kennedy, R. T. *Anal. Chem.* **2012**, *84*, 5794−5800.
(25) Nandi, P.; Desai, D. P.; Lunte, S. M. *Electrophoresis* **2010**, *31*, 1414−1422.
(26) Lucca, B. G.; Lunte, S. M.; Tomazelli Coltro, W. K.; Ferreira, V. S. *Electrophoresis* **2014**, *35*, 3363−3370.
(27) Rogers, M.; Leong, C.; Niu, X.; de Mello, A.; Parker, K. H.; Boutelle, M. G. *Phys. Chem. Chem. Phys.* **2011**, *13*, 5298−5303.
(28) Taylor, G. *Proc. R. Soc. London, Ser. A* **1953**, *219*, 186−203.
(29) Lunte, S. M.; Nandi, P.; Regel, A.; Grigsby, R.; Hulvey, M. K.; Scott, D.; Naylor, E.; Gabbert, S.; Johnson, D. In *14th International Conference on Miniaturized Systems for Chemistry and Life Sciences*; 2010; pp 1535−1537.
(30) Erkal, J. L.; Selimovic, A.; Gross, B. C.; Lockwood, S. Y.; Walton, E. L.; McNamara, S.; Martin, R. S.; Spence, D. M. *Lab Chip* **2014**, *14*, 2023−2032.
(31) Kitson, P. J.; Rosnes, M. H.; Sans, V.; Dragone, V.; Cronin, L. *Lab Chip* **2012**, *12*, 3267.
(32) Therriault, D.; White, S. R.; Lewis, J. A. *Nat. Mater.* **2003**, *2*, 265−271.
(33) Snowden, M. E.; King, P. H.; Covington, J. a; Macpherson, J. V.; Unwin, P. R. *Anal. Chem.* **2010**, *82*, 3124−3131.
(34) Anderson, K. B.; Lockwood, S. Y.; Martin, R. S.; Spence, D. M. *Anal. Chem.* **2013**, *85*, 5622−5626.

DOI: 10.1021/acs.analchem.5b01353
Anal. Chem. 2015, 87, 7763−7770

(35) Waldbaur, A.; Rapp, H.; Länge, K.; Rapp, B. E. *Anal. Methods* **2011**, *3*, 2681.
(36) Patel, B. A.; Rogers, M.; Wieder, T.; O'Hare, D.; Boutelle, M. G. *Biosens. Bioelectron.* **2011**, *26*, 2890−2896.
(37) Viggiano, A.; Marinesco, S.; Pain, F.; Meiller, A.; Gurden, H. J. *Neurosci. Methods* **2012**, *206*, 1−6.
(38) Vasylieva, N.; Barnych, B.; Meiller, A.; Maucler, C.; Pollegioni, L.; Lin, J.-S.; Barbier, D.; Marinesco, S. *Biosens. Bioelectron* **2011**, *26*, 3993−4000.
(39) Feuerstein, D.; Parker, K. H.; Boutelle, M. G. *Anal. Chem.* **2009**, *81*, 4987−4994.
(40) Heinonen, I.; Kalliokoski, K. K.; Hannukainen, J. C.; Duncker, D. J.; Nuutila, P.; Knuuti, J. *Physiology (Bethesda)* **2014**, *29*, 421−436.
(41) Timofeev, I.; Carpenter, K. L. H.; Nortje, J.; Al-Rawi, P. G.; O'Connell, M. T.; Czosnyka, M.; Smielewski, P.; Pickard, J. D.; Menon, D. K.; Kirkpatrick, P. J.; Gupta, A. K.; Hutchinson, P. J. *Brain* **2011**, *134*, 484−494.
(42) Kristensen, D. L.; Ladefoged, S. A; Sloth, E.; Aagaard, R.; Birke-Sørensen, H. *Br. J. Oral Maxillofac. Surg.* **2013**, *51*, 117−122.

DOI: 10.1021/acs.analchem.5b01353
Anal. Chem. 2015, 87, 7763−7770